176 (2023) 207538

Contents lists available at ScienceDirect

Micro and Nanostructures

journal homepage: www.journals.elsevier.com/micro-and-nanostructures

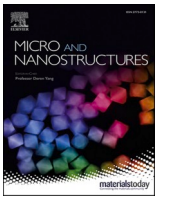

Design and fabrication process flow for high-efficiency and flexible InGaN solar cells

Rajat Gujrati [a,b], Soufiane Karrakchou [a], Lucas Oliverio [a], Suresh Sundaram [a,c,d], Paul L. Voss [a,c], Eva Monroy [e], Jean Paul Salvestrini [a,c,d,*], Abdallah Ougazzaden [a,c]

[a] CNRS, Georgia Tech – CNRS IRL 2958, 2 Rue Marconi, 57070, Metz, France
[b] Georgia Institute of Technology, Woodruff School of Mechanical Engineering, Atlanta, GA, 30332-0250, USA
[c] Georgia Institute of Technology, School of Electrical and Computer Engineering, Atlanta, GA, 30332-0250, USA
[d] Georgia Tech Europe, 2 Rue Marconi, 57070, Metz, France
[e] University Grenoble-Alpes, CEA, Grenoble INP, IRIG, PHELIQS, 17 Av. des Martyrs, Grenoble, 38000, France

ARTICLE INFO

Keywords:
InGaN nano-pyramids
Two-dimensional (2D) hexagonal boron nitride
Flexible solar cells
Optimization

ABSTRACT

We present the design of high-efficiency and flexible InGaN solar cells based on nano-pyramid absorbers, which allows for high indium incorporation and reduced polarization effects while maintaining high crystalline quality. The process uses nanoscale selective area growth and van der Waals epitaxy on two-dimensional (2D) hexagonal boron nitride on sapphire substrates. The 2D layer enables mechanical release of solar cells via self-lift-off and its transfer to a flexible substrate. Through coupled optical and electrical simulations, we compare different designs of the p- and n-regions and propose two device architectures that combine mechanical flexibility and high power conversion efficiency (up to 16.4%). This approach can provide a solution for the fabrication of high-efficiency, low-cost and flexible InGaN-based solar cells.

1. Introduction

The rapid development of wearable and flexible electronics has increased the need for high-efficiency, robust, low-cost and flexible photovoltaic devices [1]. III-V thin-film solar cells are promising candidates for these applications owing to advancements in epitaxial growth and lift-off of III-V semiconductors. Laser lift-off [2], chemical lift-off [3] and mechanical spalling [4] allow for efficient release of III-V epilayers, e.g. GaAs [5] and InP [6] based structures, from the native substrate and their transfer onto lightweight and flexible receiving [7] substrates.

InGaN alloys have outstanding photovoltaic properties such as a high absorption coefficient, a tunable band gap that covers nearly the entire solar spectrum, and resistance to high temperatures and high energy radiation [8]. Moreover, InGaN-based solar cells can be grown by van der Waals epitaxy on two-dimensional (2D) hexagonal boron nitride (h-BN) on sapphire [9], which allows for a 2D-layer-assisted transfer [10] to foreign substrates [11]. [12] This emerging approach could offer a number of important advantages over conventional lift-off techniques, including the possibility to grow 2D h-BN and InGaN-based solar cells in a single epitaxial run, while the sapphire substrate can be reused repeatedly after the mechanical release of the III-nitride epilayers [13].

However, the roadmap to achieve high-efficiency InGaN solar cell is impeded by two primary challenges. First, degradation of crystalline quality and phase separation at large layer thickness and high indium content respectively [14]. Second, strong polarization

* Corresponding author. CNRS, Georgia Tech – CNRS IRL 2958, 2 rue Marconi, 57070, Metz, France.
E-mail address: jean-paul.salvestrini@georgiatech-metz.fr (J.P. Salvestrini).

https://doi.org/10.1016/j.micrna.2023.207538
Received 5 December 2022; Accepted 22 January 2023
Available online 18 February 2023

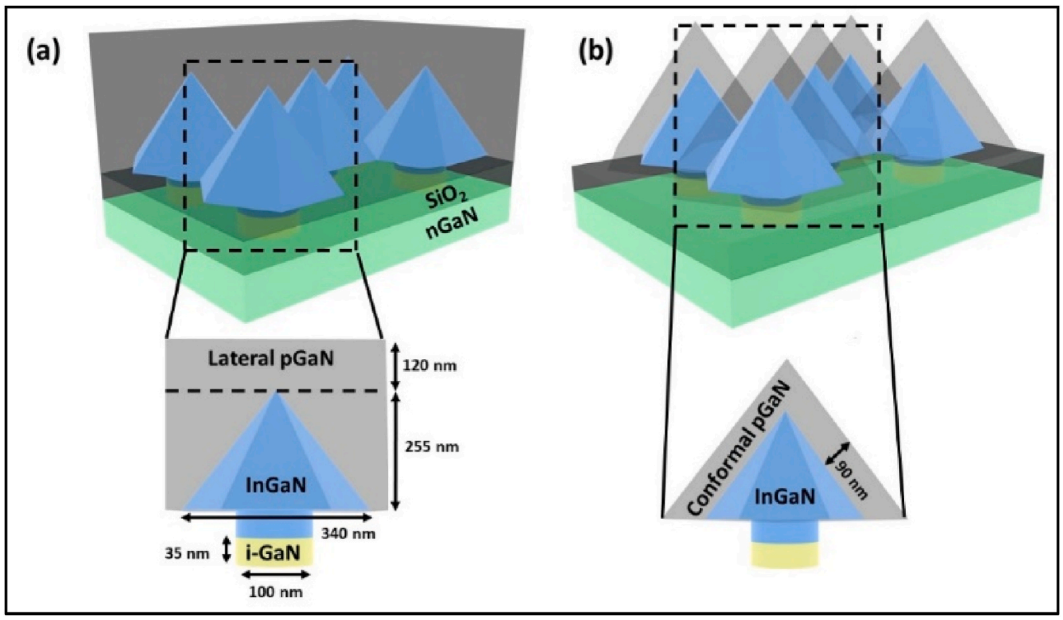

Fig. 1. Schematics of (a) NP-L (lateral p-GaN) and (b) NP-C (conformal p-GaN) solar cells design.

charges [15] at InGaN/GaN hetero-interface, which reduces the build-in electric field required for carrier separation [16]. To tackle these challenges, InGaN solar cells with different planar absorber layers including InGaN superlattice [17], semibulk [18] and multi-quantum wells [19] and most recently, n [20] on p structure [21], which could benefit from interface polarization charges, have been proposed. Yet, due to above-mentioned issues, the highest experimentally achieved power conversion efficiency (PCE) is below 6% with indium content of 19% [22]. Thus, new approaches are required to achieve InGaN solar cells of higher indium composition while managing the lattice mismatch between the absorber layer and the substrate and contact layers.

Three-dimensional (3D) nanostructures are promising candidates to obtain high-crystalline quality, indium rich InGaN material, where the misfit strain is elastically released, thanks to the high surface-to-volume ratio during growth. InGaN nano-pyramids (NPs) grown by nano-selective area growth (NSAG) [23] allow elastic strain relaxation of InGaN, which results in defect-free absorber material with indium content up to 33% [24]. In addition to the enhanced indium incorporation, these InGaN NPs reduce the effects of piezoelectric and spontaneous polarization since the material grows along the semipolar <1–102> r-plane facets of the pyramids. Considering this, El-Huni et al. [25] proposed the idea of NP shaped InGaN absorber layers. Through simulations, they optimized the shape of these NPs for efficient light trapping and showed that these nanostructures can lead to an enhancement of the conversion efficiency, up to twice that of conventional planar InGaN-based solar cells.

The challenge however, with these InGaN NP solar cells is the degradation of the InGaN absorber during the growth of the p-GaN top layer. Using metal-organic vapor phase epitaxy (MOVPE), high p-GaN growth temperature above 850 °C leads to indium segregation in the InGaN absorber [26]. On the other hand, when the p-GaN epitaxial layer is grown by MOVPE at low temperature, the crystal quality of p-GaN is degraded, leading to high carrier recombination and leakage current [19]. [27] The solution used to overcome this issue is to grow p-GaN layer under epitaxial lateral overgrowth conditions, which allows reduction of the thermal budget on the absorber layer, thanks to the higher growth rate [28]. Such growth conditions prevent the degradation of the NPs, but leads to poorly doped and highly resistive planarization layer between absorber NP and p-GaN.

A solution that we propose in this work, is the low temperature growth of p-GaN layer on NPs by molecular beam epitaxy (MBE). Several studies have reported high-quality growth of p-GaN by MBE at low temperature (~700 °C) [29], thus ensuring preserved InGaN [30] absorber underneath. However, unlike the lateral structure of NP solar cells grown by MOVPE (referred as NP-L and illustrated in Fig. 1(a)), MBE grown p-GaN will lead to conformal NP solar cells (referred as NP-C and shown in Fig. 1(b)). This means, the two structures differ from one another from the perspective of light coupling into the structure. Through coupled optical and electrical simulations we show that, our proposed solution, NP-C design leads to a significant reduction of the reflectivity of the top surface. This increases the overall PCE by ~100% as compared to the NP-L design. Further optimization of the NP-C design is achieved by replacing the n-GaN layer by an n-$In_yGa_{1-y}N$ layer to reduce both the polarization charge effect and electron transport barrier at the InGaN/n-GaN interface, leading to an additional increase of the PCE by 41%.

Finally, for the fabrication of flexible solar cells, we propose to use the very recently developed self-lift-off and transfer (SLOT) process. This technology has been used for the development of flexible LEDs [31]. The method involves the deposition of a 30 μm thick copper layer on the solar cell structure grown on 2D h-BN/sapphire substrate. Thanks to the weak van der Waals force between h-BN and sapphire, the epilayers are lifted off at h-BN/sapphire interface and transferred to copper upon application of thermomechanical stress. Transfer of NP-C structure to thin copper substrates in addition to giving flexibility would facilitate vertical transport, heat

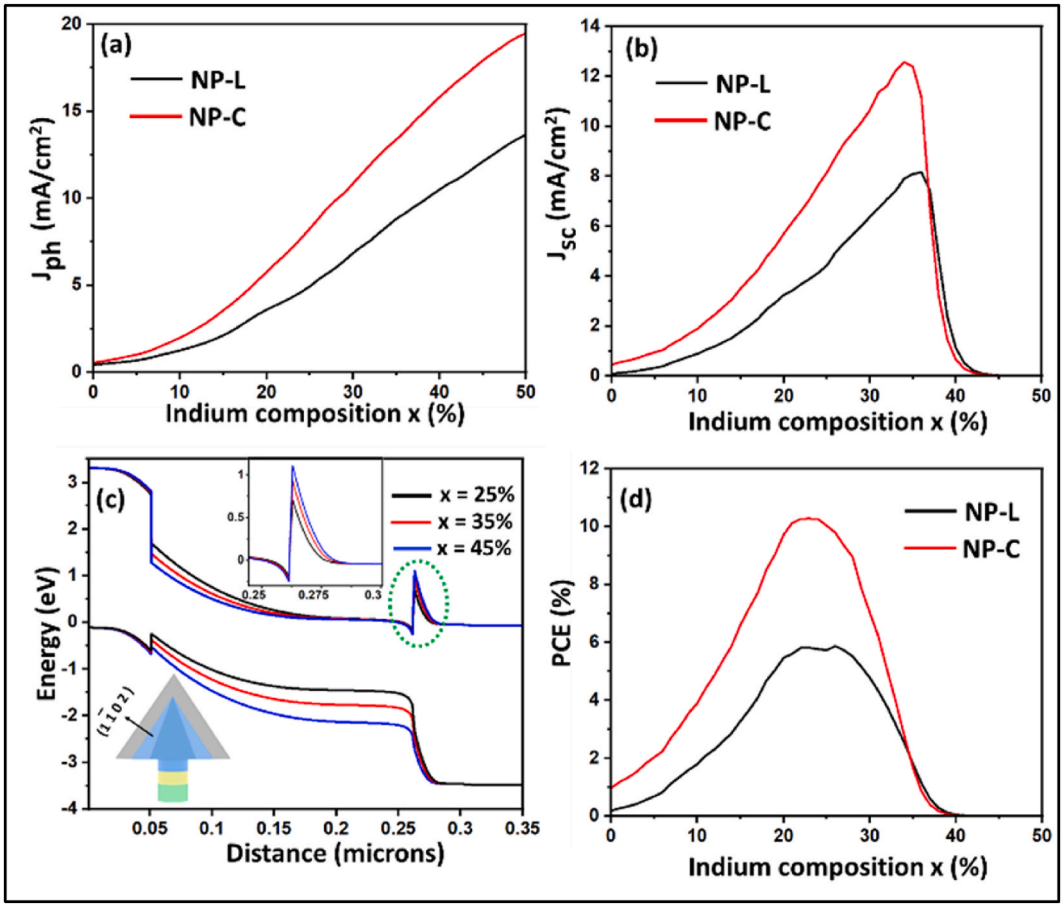

Fig. 2. **(a)** Plot of ideal J_{ph} (mA/cm^2) vs Indium content (x) **(b)** J_{sc} (mA/cm^2) vs, Indium content (x) **(c)** Band diagram of the NP-C structure for x = 25%, 35% and 45% calculated along the ⊥(1–102) direction, as shown in schematic. The inset is a zoomed view of the potential barrier in the conduction band that appears at the InGaN/n-GaN interface (outlined by a green dashed ellipse), at the base of the pyramid. **(d)** Plot of PCE (%) vs indium content (x).

removal, and the creation of electrical pads and backside mirrors. Using this technology, we describe the fabrication process flow of two new architectures of flexible solar cells referred to as NPC-on-Cu (Fig. 5(d)) and NPC-free-standing (Fig. 5(f)). Through simulations, we show that both NPC-on-Cu and NPC-free-standing architectures can achieve PCE as high as 14.8% and 16.5%, respectively.

2. Methods

Both NP-L and NP-C designs (Fig. 1) are p-GaN/InGaN/n-GaN Ga-face heterojunctions where the n-layer is 50-nm-thick and Si-doped with electron concentration of 8×10^{18} cm^{-3} whereas the p-type layer is Mg-doped with hole concentration of 5×10^{17} cm^{-3}. The p-layer has a thickness of 120 nm and 90 nm for NP-L and NP-C designs, respectively (see geometric description in Fig. 1). These thicknesses were optimized to allow for minimum reflection at the p-GaN/air interface. The InGaN NPs geometric parameters were optimized elsewhere [25] and are kept same for both structures. They have a base diameter of 340 nm and a height of 255 nm, and their distribution is hexagonal close packed, so that the base of each pyramid is in contact with the base of its 6 next-neighbors. The NP stem is originated by selective area growth on a 80-nm-thick SiO_2 mask. The growth starts with a 35-nm-thick i-GaN seed layer, followed by InGaN layer of the desired indium composition. The residual donor concentration in the NPs is 1×10^{17} cm^{-3}. All these doping levels are realistic parameters considering the challenging constraints to attain high levels of p-doping in GaN.

The 3D Finite-Difference Time-Domaine (FDTD) method embedded in the Lumerical software was used to investigate matter-light interaction. The absorption coefficient and refractive index were calculated using Brown's [32] and Adachi's [33] models, respectively. We assumed that each photon absorbed leads to the generation of one electron-hole pair. The photogeneration rate, G(x, y, z) (in cm^{-3}s^{-1}), is calculated under AM 1.5 solar spectrum conditions. The ideal photocurrent density, J_{ph} (mA/cm^2 (without considering transport and recombination) is calculated as $J_{ph} = (q \iiint G(x, y, z)\, dx\, dy\, dz)/A$, where q is unit electronic charge and A is the surface area of solar cell receiving illumination.

The output photogeneration rate of 3D optical simulations is averaged along the y-axis and used as the input for electrical 2D

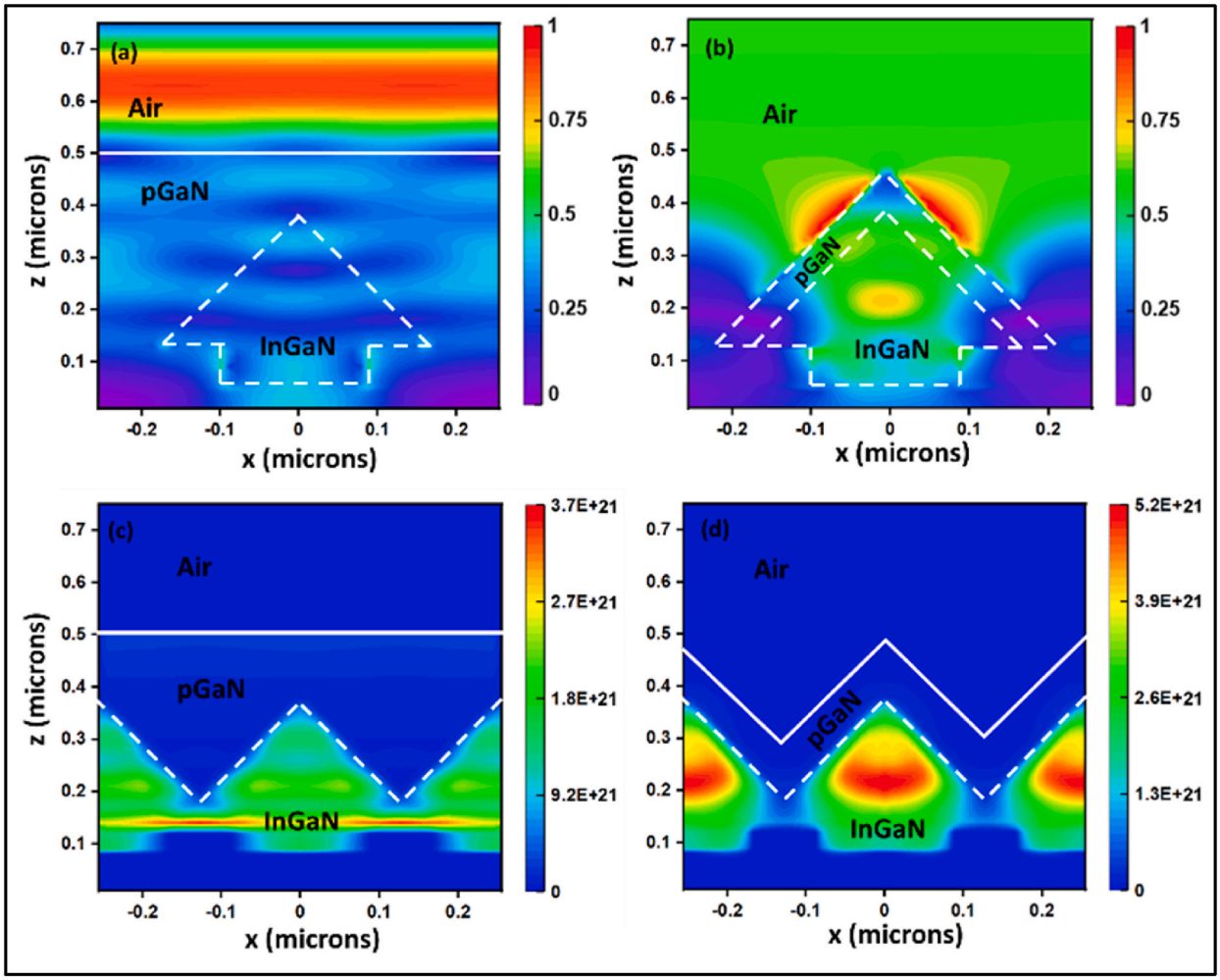

Fig. 3. Cross-section (x, z) maps of the normalized optical electric field intensity obtained at x = 30% and λ = 525 nm for (a) NP-L and (b) NP-C structures. Optical absorption has not been taken into account to clearly highlight the light trapping effect. Photogeneration rate maps ($cm^{-3}.s^{-1}$) averaged along the y-axis for (c) NP-L and (d) NP-C at x = 30%.

Silvaco TCAD simulations, allowing the calculation of the real photocurrent density J_{sc} and PCE. For that, Poisson's and current continuity equations are solved self consistently. Cauchy's carrier mobility model alongside SRH, optical and surface recombination models are also considered in our simulations. Carrier lifetime for both electrons and holes is considered to be 5ns. The polarization-induced charges at the c-plane and r-plane hetero-interfaces are computed using Romanov's model [34]. Extensive details about the physical models and material parameters used can be found in Ref. [35].

3. Results and discussion

3.1. Optimization of the NP-based InGaN solar cells

The ideal photocurrent density, J_{ph}, for the NP-L and NP-C designs [25] is calculated as a function of the indium content (x) in the NPs, with x ranging from 0 to 50% (Fig. 2). We limit our simulations only up to x = 50% due to growth constraint of higher indium content InGaN. For both designs, J_{ph} increases with indium content due to the corresponding decrease of the InGaN bandgap, which results in a better coverage of the solar spectrum. However, the photocurrent is higher in the NP-C case for all indium contents. As an example, at x = 25%, J_{ph} of NP-L is equal to 6 mA/cm^2 while it reaches 9 mA/cm^2 for NP-C, corresponding to an increase of 50%.

The improvement originates from the significant reduction of the optical reflection in the textured sample (NP–C) with respect to the planar sample (NP-L), which leads to improved coupling of the light into the NP-C structure, as illustrated in Fig. 3(a) and (b), which show cross-section maps of the optical electric field at λ = 525 nm. For the NP-L design, the light is not confined in the NPs, but rather distributed between the NPs and the p-type GaN layer. This is due to the small contrast of refractive index between GaN and InGaN. The improved optical coupling in NP-C results in enhanced photogeneration, as displayed in Fig. 3(c) and (d).

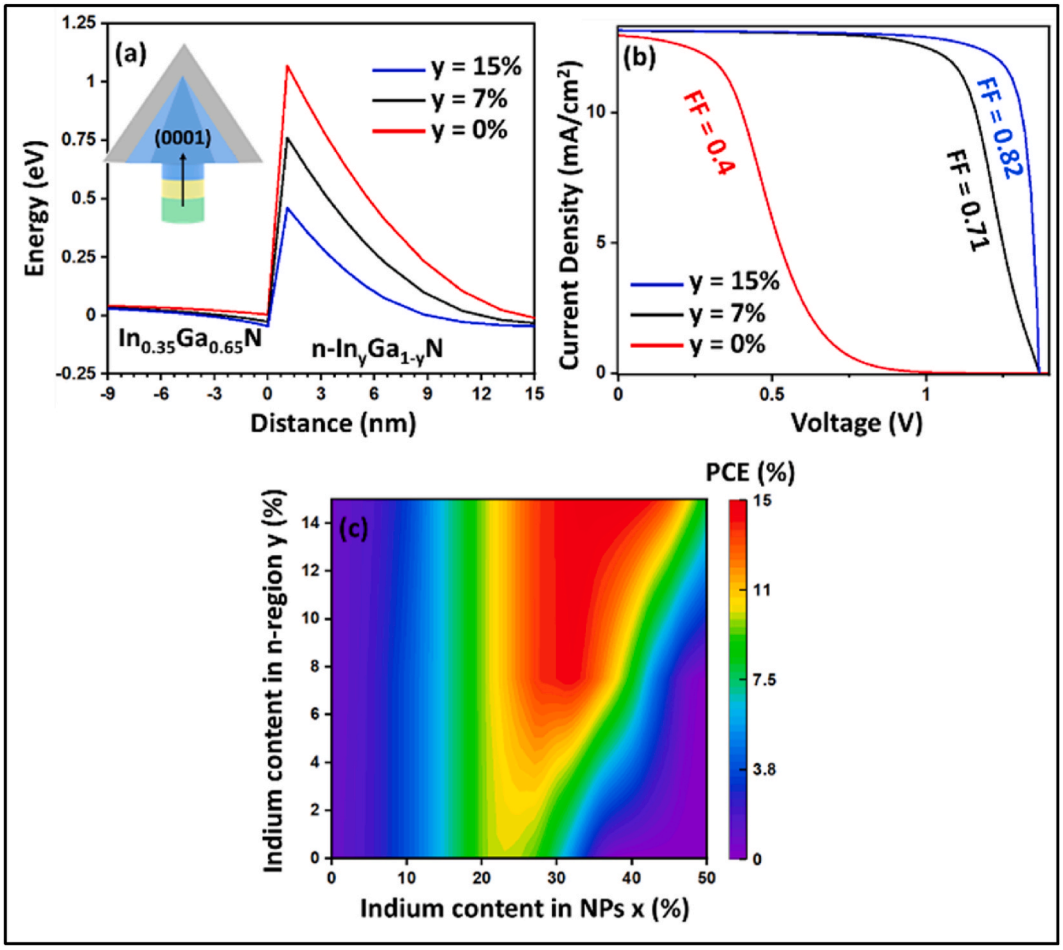

Fig. 4. (a) Conduction band at the hetero-junction along the line in [0001] direction as shown in schematic, (b) J–V characteristics under AM1.5 illumination for the p-GaN/$In_{0.35}Ga_{0.65}N$/n-$In_yGa_{1-y}N$ NP-C structure and (c) PCE with respect to Indium content in NPs (x) and n-region (y).

The photogeneration rate obtained is used as an input for electrical simulations. The short-circuit current density (J_{sc}) and the power conversion efficiency (PCE) of the NP-L and NP-C solar cells are computed as a function of the Indium content in the NPs, ranging from 0 to 50%. Fig. 2(b) shows J_{sc} versus x for both designs. The value of J_{sc} increases with the Indium content and reaches a peak value of 8.2 mA/cm^2 at x = 36% for NP-L and 12.5 mA/cm^2 at x = 34% for NP-C. The maximum J_{sc} obtained in the case of NP-C is 53% higher than in case of NP-L. After attaining maxima, J_{sc} drops for higher Indium contents, which is attributed to the increase of polarization effects as well as the increasing band offset at the InGaN/n-GaN hetero-interface. Therefore, photogeneration keeps increasing at high Indium concentrations, but the resulting charge carriers are not collected at the contacts.

Fig. 2(c) shows the energy band diagram of the NP structure for x = 0.25, 0.35 and 0.45. The horizontal axis corresponds to the relative distance along the cutline drawn perpendicular to the r(1–102) plane face of the pyramid from p region to all the way down to the bottom n-region. This is chosen as the current flow is perpendicular to the inclined facets of the pyramids and not along the axis of the pyramids. We observe the presence of a potential barrier for electrons at the $In_{0.35}Ga_{0.65}N$/n-GaN interface (outlined by a green dashed ellipse in the figure), which increases with the indium content in the absorber. Furthermore, the band bending along the InGaN region, due to the presence of the junction, is attenuated for increasing indium content due to the higher polarization-induced field, which is in the opposite direction of the built-in electric field in the case of p-i-n Ga-face structures [16]. This limits the drift of the carriers to the n- and p-layers. The PCE versus indium content is given in Fig. 2(d) for the NP-L and NP-C designs. The maximum efficiency for NP-L and NP-C is equal to 5.9% and 10.3%, respectively, and is attained for an indium content of ~23% for both the designs. The efficiency drops abruptly for higher indium contents as a result of the transport limitations.

These results confirm the superior photovoltaic behavior of the NP-C design compared to the NP-L one, owing to the higher light absorption that is enhanced by the textured pyramid-shaped p-GaN top-surface. However, the electrical performance of this structure is still hindered by the polarization-induced charges and the high barrier height at the InGaN/n-GaN hetero-interface. Thus, we study the effect of replacing the n-GaN layer by an n- $In_yGa_{1-y}N$ layer, with the same doping concentration of 8×10^{18} cm^{-3}, on the overall efficiency of the NP-C structure.

In the following, the n-GaN layer below the SiO_2 mask is replaced by a 50-nm-thick n-$In_yGa_{1-y}N$ layer, where y is varied from 0% to

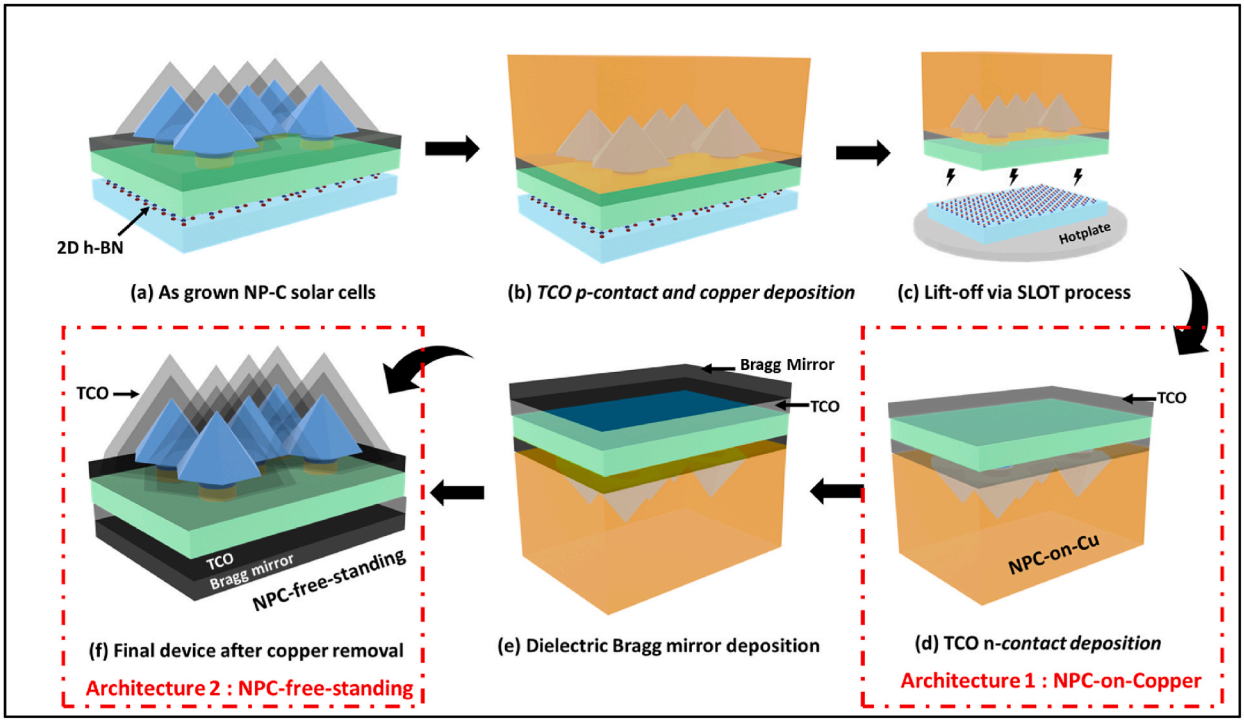

Fig. 5. Schematics of the SLOT process steps for the fabrication of flexible InGaN solar cells with both NPC-on-Cu and NPC-free-standing device architectures.

15%. Fig. 4(a) shows the conduction band profile at the interface between the NP base and the n-$In_yGa_{1-y}N$ layer, to illustrate the effect of increasing the indium content (y) in the n-$In_yGa_{1-y}N$ layer on the electron potential barrier. For a fixed indium content in the NP (x = 0.35), the barrier height decreases from 1.1 eV for (y = 0) to 0.46 eV (for y = 0.15). Fig. 4(b) shows the resulting improvement in the J-V characteristics under AM1.5 illumination, and Fig. 4(c) gives the dependence of the PCE on the x and y indium mole fractions. Increasing the indium content in the n-region results in a lower potential barrier for the electrons due to the lower polarization difference at the interface. As a result, the carrier collection efficiency improves. This has a direct effect in the J-V curves, where the fill factor (FF) increases from 0.4 for y = 0% to 0.71 and 0.82 for y = 7% and 15%, respectively. A maximum PCE of 14.6% is reached at x = 32% and y = 7%, while the maximum PCE obtained for y = 0 is equal to 10.8% (at x = 23%), which correspond to an increase of 35% in efficiency. A slightly higher PCE is reached in the region where x is higher than 32% and y higher than 7%.

Note that all the results presented above are obtained by considering a 50-nm-thick n-region. This thickness is below the critical thickness for both n-GaN and n-$In_{0.07}Ga_{0.83}N$, hence such layers can be grown with high crystalline quality. However, the material quality of n-$In_{0.15}Ga_{0.85}N$ is severely degraded when the thickness reaches a critical value ~20 nm [36]. Considering this experimental challenge and the limited improvement of the PCE for x higher than 32% and y higher than 7%, we consider than an optimized and realistic InGaN NP-based solar cell device should include: (i) pyramid-shaped p-GaN region, (ii) an $In_{0.32}Ga_{0.68}N$ NP absorber layer and (iii) n-$In_{0.07}Ga_{0.93}N$ region.

3.2. *Design of flexible NPC-based solar cells*

The process flows to fabricate two new architectures of flexible solar cells through the SLOT process are shown in Fig. 5. The first architecture (referred as NPC-on-Cu and illustrated in Fig. 5(d)) is obtained via the deposition of transparent conductive oxide (TCO) as p-contact, followed by deposition of copper layer (Fig. 5(b)). Then, the process is completed by the release of the active structure via the SLOT process (Fig. 5(c)), and the deposition of a TCO n-contact layer on the flipped membrane (Fig. 5(d)). The second architecture (referred as NPC-free-standing and presented in Fig. 5(f)) is obtained from the NPC-on-Cu structure by the deposition of a dielectric Bragg mirror on top of the TCO n-contact followed by a selective etching of the copper layer to allow fully transparent, free-standing and flexible InGaN solar cell (Fig. 5(f)).

Using the same simulation approach, we investigate here the optical and electrical performance of flexible NPC-on-Cu (Fig. 5(d)) and NPC-free-standing devices (Fig. 5(f)). The TCO layer is considered to be indium zinc oxide (IZO) because it allows higher electrical conductivity [37] and mechanical flexibility [38] when compared to indium tin oxide (ITO).

For the NPC-on-Cu device without IZO n-contact, large optical confinement is obtained close to the SiO_2 mask (not shown in manuscript). This effect is due to the larger refractive index contrast at the $In_{0.32}Ga_{0.68}N/SiO_2$ and n-$In_{0.07}Ga_{0.93}N/SiO_2$ interfaces, as well as the copper back-mirror effect. However, the flat n-layer on top of the structure increases the reflectivity with respect to the NP-C

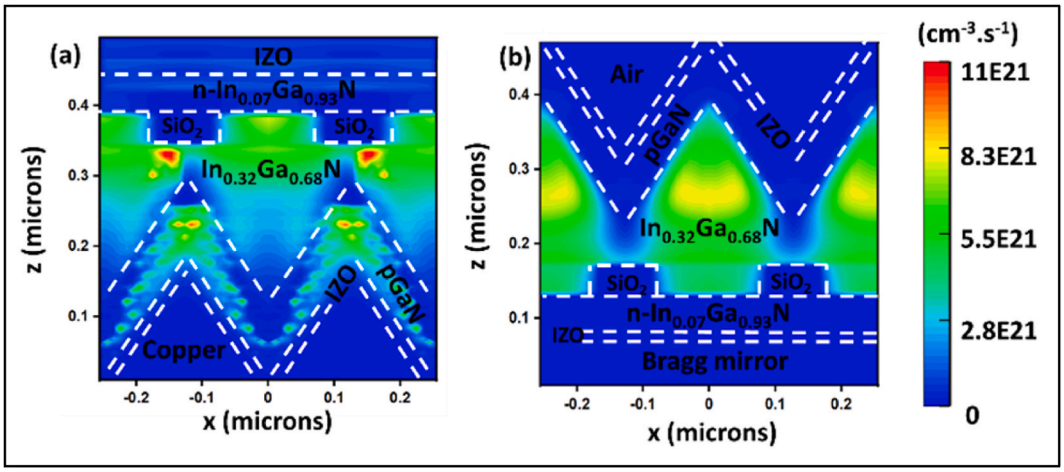

Fig. 6. Photogeneration map (x, z) averaged along the y-axis of (a) the NPC-on-Cu architecture with IZO, (b) the NPC-free-standing architecture with IZO and Bragg mirror.

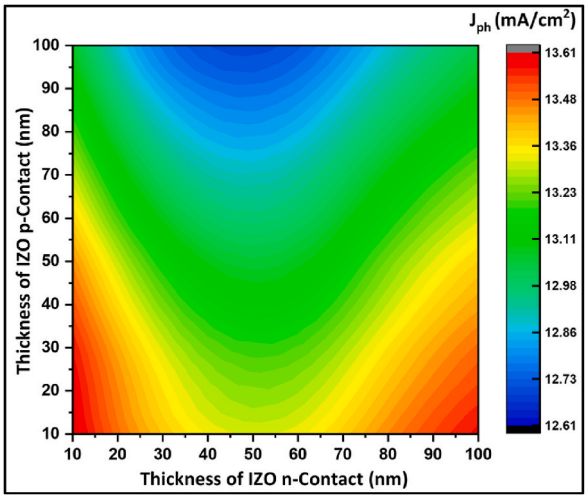

Fig. 7. Ideal photocurrent density, J_{ph} (mA/cm^2) as a function of the IZO contact thickness for the NPC-free-standing architecture.

structure, hence reducing the absorption within the NPs. Moreover, the 50-nm-thick n-$In_{0.07}Ga_{0.93}N$ layer absorbs around 18% of the solar spectrum, which further limits the amount of light reaching the NPs. These constraints lead to a of $J_{sc} = 8.8$ mA/cm^2, which is 23% lower than the $J_{sc} = 11.4$ mA/cm^{2}obtained for the NP-C structures. The PCE also drops from 14.6% for the NP-C to 10.5% for the NPC-on-Cu device.

The performance of NPC-on-Cu device, in terms of absorption and photogeneration, can be enhanced by depositing a 60-nm-thick (optimized thickness) IZO n-contact layer, which behaves as anti-reflective coating. The photogeneration rate is illustrated in Fig. 6(a). Ultimately, the IZO/NPC-on-Cu structure reaches a maximum J_{sc} of 12.4 mA/cm^2 and a maximum PCE of 14.8%.

For the NPC-free-standing architecture, 6 periods of SiN (50 nm)/SiO_2 (100 nm) are used as Bragg reflector in the wavelength range from 500 nm to 700 nm. Furthermore, thickness of both IZO p- and n-contacts affects the ideal photocurrent density J_{ph}, which varies periodically (period ≈ 100 nm) with the thickness of the IZO n-contact and decreases monotonically with the thickness of the IZO p-contact, as illustrated in Fig. 7. Thus, an optimal thickness of 10 nm is used for both IZO p- and n-contacts. With these parameters, the NPC-free-standing device with IZO contacts and back mirror presents an improved photogeneration within the NPs (Fig. 6(b)) and can reach $J_{sc} = 13.3$ mA/cm^2 ($J_{ph} = 13.6$ mA/cm^2) and PCE = 16.5%. The fact that the values of J_{sc} and J_{ph} are so close is explained by the high charge collection efficiency of photogenerated carriers. This is realistic since the potential barrier for hole transport is relatively small (Fig. 2(c)) and, the potential barrier for electron transport at the InGaN NP/n-$In_{0.07}Ga_{0.93}N$ interface is narrow (<9 nm in Fig. 4 (a)), so that electrons can tunnel through.

Table 1
Summary of the J_{sc} and PCE values obtained for different solar cell structures.

	NP-L with n-GaN	NP-C with n-GaN	NP-C with n-$In_{0.07}Ga_{0.93}N$	NPC-on-Cu device	NPC-free-standing device
	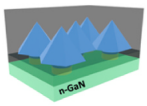	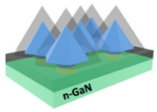	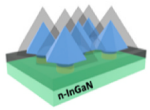	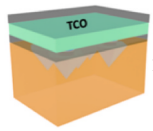	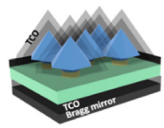
Optimal Indium content (%)	23	23	32	32	32
J_{sc} (mA/cm^2)	3.8	7.1	11.4	12.4	13.3
PCE (%)	5.9	10.3	14.6	14.8	16.5

Table 2
Comparison of the state-of-the-art with results obtained in this work.

Reference	Structure	PCE
El. Huni et al. [25]	NPs, lateral p-GaN, In = 30% (+ TCO and BM)	10.80%
This work	NPs, conformal p-GaN, In = 32% (+ TCO and BM)	16.50%
Kazazis et al. [21]	Planar absorber, n on p structure, In = 50%.	14.5%
This work	NP absorber, conformal p-GaN In = 32%	14.6%

4. Conclusion

The results obtained in this study and summarized in Table 1, show that the p-GaN-conformal NP-C structure exhibits higher PCE than the planar NP-L structure due to the improved optical coupling and higher optical absorption in the NP region. Moreover, by replacing the n-GaN layer by n-$In_{0.07}Ga_{0.93}N$, to improve the carrier transport, we demonstrate that an optimized and experimentally feasible p-GaN/$In_{0.32}Ga_{0.68}N$/n-$In_{0.07}Ga_{0.93}N$ NP-C structure on sapphire can attain a PCE of 14.6%. It should be noted that this value is almost equal the best reported PCE (14.5%) obtained by simulation for bulk InGaN/GaN solar cells [21] consisting of an ideal 300-nm-thick $In_{0.5}Ga_{0.5}N$ layer grown on p-GaN. This structure [21] however efficient, is infeasible to realize owing to two reasons. On the one hand, the thickness of $In_{0.5}Ga_{0.5}N$ is far beyond its critical thickness on GaN, which results in layers with inhomogeneous composition (strain pulling effect) and with a high density of structural defects. On the other side, n-side-up devices present additional difficulties for the activation of Mg, since the subsequent regrowth of n-GaN does not allow an efficient decomposition of the hydrogen complexes formed in the Mg-doped layer [39]. Our proposed solution based on NPs eliminate the intrinsic challenges in the state-of-the-art structure.

The solar cells described in this study can be grown and fabricated on 2D h-BN/sapphire substrates, which allows the mechanical release of the epilayer, and its transfer to flexible substrates. This target can be reached through the one-step self-lift-off and transfer (SLOT) process where a thick copper layer is deposited on the top-surface to trigger the release of the epilayers at the h-BN/sapphire interface under thermo-mechanical stress. This process results in inverted n-on-top flexible solar cells on copper. We demonstrate that the photovoltaic performance of these NPC-on-Cu devices are penalized by the lack of top-surface texturing and partial light absorption in the n-$In_{0.07}Ga_{0.93}N$ top layer, with results in a PCE limited to 10.4%. However, by adding an optimized IZO n-contact layer that also acts as ARC, the PCE in such solar cells can be 14.8%. A second design architecture is also proposed and is based on the deposition of a Bragg mirror on the n-side and the selective removal of copper from the p-side to allow free-standing and flexible p-on-top NPC-free-standing devices. It leads to a maximum PCE of 16.5%. PCE obtained in this study is compared with the state-of-the-art results and is presented in Table 2.

Finally, it is worth mentioning that the high thermal dissipation capability of copper can make the NPC-on-Cu devices more suitable for high temperature applications, whereas the NPC-free-standing devices can be more adapted for heterogeneous integration on Si-based solar cells in order to achieve high-efficiency 4-terminal [35] and 3-terminal [40] tandem cells.

Credit author statement

Rajat Gujrati: Investigation, Visualization, Writing-original draft. **Soufiane Karrakchou & Eva Monroy:** Visualization, Writing – review & editing. **Lucas Oliverio:** Methodology, Validation. **Suresh Sundaram and Paul L. Voss:** Resources. **Jean Paul Salvestrini & Abdallah Ougazzaden:** Conceptualization, Funding acquisition, Project administration, Supervision, Writing – review & editing.

Declaration of competing interest

The authors declare that they have no known competing financial interests or personal relationships that could have appeared to

influence the work reported in this paper.

Data availability

Data will be made available on request.

Acknowledgement

This study has been funded by the French National Research Agency (ANR), under the INMOST (Grant ANR-19-CE08-0025) project, and French PIA project Lorraine Université d'Excellence (Grant ANR-15- IDEX-04-LUE), as well as by the Region Grand Est. We also thank Dr. Walid El. Huni (Infineon Technologies, Austria) for fruitful discussions on simulations.

References

[1] X. Li, P. Li, Z. Wu, D. Luo, H. Yu, Z. Lu, Review and perspective of materials for flexible solar cells, Mater. Reports Energy. 1 (2021), 100001, https://doi.org/10.1016/j.matre.2020.09.001.
[2] R. Delmdahl, R. Pätzel, J. Brune, Large-area laser-lift-off processing in microelectronics, Phys. Procedia (2013) 241–248, https://doi.org/10.1016/j.phpro.2013.03.075.
[3] W. Choi, C.Z. Kim, C.S. Kim, W. Heo, T. Joo, S.Y. Ryu, H. Kim, H. Kim, H.K. Kang, S. Jo, A repeatable epitaxial lift-off process from a single GaAs substrate for low-cost and high-efficiency III-V solar cells, Adv. Energy Mater. 4 (2014), 1400589, https://doi.org/10.1002/aenm.201400589.
[4] S.W. Bedell, D. Shahrjerdi, B. Hekmatshoar, K. Fogel, P.A. Lauro, J.A. Ott, N. Sosa, D. Sadana, Kerf-less removal of Si, Ge, and III-V layers by controlled spalling to enable low-cost PV technologies, IEEE J. Photovoltaics 2 (2012) 141–147, https://doi.org/10.1109/JPHOTOV.2012.2184267.
[5] M.C. Tseng, R.H. Horng, Y.L. Tsai, D.S. Wuu, H.H. Yu, Fabrication and characterization of GaAs solar cells on copper substrates, IEEE Electron. Device Lett. 30 (2009) 940–942, https://doi.org/10.1109/LED.2009.2026292.
[6] K.T. Shiu, J. Zimmerman, H. Wang, S.R. Forrest, Ultrathin film, high specific power InP solar cells on flexible plastic substrates, Appl. Phys. Lett. 95 (2009) 4–7, https://doi.org/10.1063/1.3268805.
[7] J. Yoon, S. Jo, I.S. Chun, I. Jung, H.S. Kim, M. Meitl, E. Menard, X. Li, J.J. Coleman, U. Paik, J.A. Rogers, GaAs photovoltaics and optoelectronics using releasable multilayer epitaxial assemblies, Nature 465 (2010) 329–333, https://doi.org/10.1038/nature09054.
[8] J. Wu, W. Walukiewicz, K.M. Yu, W. Shan, J.W. Ager, E.E. Haller, H. Lu, W.J. Schaff, W.K. Metzger, S. Kurtz, Superior radiation resistance of In1−xGaxN alloys: full-solar-spectrum photovoltaic material system, J. Appl. Phys. 94 (2003) 6477–6482, https://doi.org/10.1063/1.1618353.
[9] Y. Kobayashi, K. Kumakura, T. Akasaka, T. Makimoto, Layered boron nitride as a release layer for mechanical transfer of GaN-based devices, Nature 484 (2012) 223–227, https://doi.org/10.1038/nature10970.
[10] T. Ayari, S. Sundaram, X. Li, Y. El Gmili, P.L. Voss, J.P. Salvestrini, A. Ougazzaden, Wafer-scale controlled exfoliation of metal organic vapor phase epitaxy grown InGaN/GaN multi quantum well structures using low-tack two-dimensional layered h-BN, Appl. Phys. Lett. 108 (2016), 171106, https://doi.org/10.1063/1.4948260.
[11] T. Ayari, S. Sundaram, X. Li, S. Alam, C. Bishop, W. El Huni, M.B. Jordan, Y. Halfaya, S. Gautier, P.L. Voss, J.P. Salvestrini, A. Ougazzaden, Heterogeneous integration of thin-film InGaN-based solar cells on foreign substrates with enhanced performance, ACS Photonics 5 (2018) 3003–3008, https://doi.org/10.1021/acsphotonics.8b00663.
[12] S. Karrakchou, S. Sundaram, T. Ayari, A. Mballo, P. Vuong, A. Srivastava, R. Gujrati, A. Ahaitouf, G. Patriarche, T. Leichlé, S. Gautier, T. Moudakir, P.L. Voss, J. P. Salvestrini, A. Ougazzaden, Effectiveness of selective area growth using van der Waals h-BN layer for crack-free transfer of large-size III-N devices onto arbitrary substrates, Sci. Rep. 10 (2020), 21709, https://doi.org/10.1038/s41598-020-77681-z.
[13] K. Qiao, Y. Liu, C. Kim, R.J. Molnar, T. Osadchy, W. Li, X. Sun, H. Li, R.L. Myers-Ward, D. Lee, S. Subramanian, H. Kim, K. Lu, J.A. Robinson, W. Kong, J. Kim, Graphene buffer layer on SiC as a release layer for high-quality freestanding semiconductor membranes, Nano Lett. 21 (2021) 4013–4020, https://doi.org/10.1021/acs.nanolett.1c00673.
[14] Y. El Gmili, G. Orsal, K. Pantzas, A. Ahaitouf, T. Moudakir, S. Gautier, G. Patriarche, D. Troadec, J.P. Salvestrini, A. Ougazzaden, Characteristics of the surface microstructures in thick InGaN layers on GaN, Opt. Mater. Express 3 (2013) 1111, https://doi.org/10.1364/ome.3.001111.
[15] A.G. Bhuiyan, K. Sugita, A. Hashimoto, A. Yamamoto, InGaN solar cells: present state of the art and important challenges, IEEE J. Photovoltaics 2 (2012) 276–293, https://doi.org/10.1109/JPHOTOV.2012.2193384.
[16] K. Wang, Q. Wang, J. Chu, H. Xiao, X. Wang, Z. Wang, Roles of polarization effects in InGaN/GaN solar cells and comparison of p-i-n and n-i-p structures, Opt Express 26 (2018) A946, https://doi.org/10.1364/oe.26.00a946.
[17] Jinn-Kong Sheu, Chih-Ciao Yang, Shang-Ju Tu, Kuo-Hua Chang, Ming-Lun Lee, Wei-Chih Lai, Li-Chi Peng, Demonstration of GaN-based solar cells with GaN/inGaN superlattice absorption layers, IEEE Electron. Device Lett. 30 (2009) 225–227, https://doi.org/10.1109/LED.2008.2012275.
[18] M. Arif, W. Elhuni, J. Streque, S. Sundaram, S. Belahsene, Y. El Gmili, M. Jordan, X. Li, G. Patriarche, A. Slaoui, A. Migan, R. Abderrahim, Z. Djebbour, P.L. Voss, J.P. Salvestrini, A. Ougazzaden, Improving InGaN heterojunction solar cells efficiency using a semibulk absorber, Sol. Energy Mater. Sol. Cells 159 (2017) 405–411, https://doi.org/10.1016/j.solmat.2016.09.030.
[19] C.J. Neufeld, N.G. Toledo, S.C. Cruz, M. Iza, S.P. DenBaars, U.K. Mishra, High quantum efficiency InGaN/GaN solar cells with 2.95 eV band gap, Appl. Phys. Lett. 93 (2008) 91–94, https://doi.org/10.1063/1.2988894.
[20] A. Mukhtarova, S. Valdueza-Felip, L. Redaelli, C. Durand, C. Bougerol, E. Monroy, J. Eymery, Dependence of the photovoltaic performance of pseudomorphic InGaN/GaN multiple-quantum-well solar cells on the active region thickness, Appl. Phys. Lett. 108 (2016), https://doi.org/10.1063/1.4947445.
[21] S.A. Kazazis, E. Papadomanolaki, E. Iliopoulos, Polarization-engineered InGaN/GaN solar cells: realistic expectations for single heterojunctions, IEEE J. Photovoltaics 8 (2018) 118–124, https://doi.org/10.1109/JPHOTOV.2017.2775164.
[22] B.W. Liou, Design and fabrication of InxGa1−xN/GaN solar cells with a multiple-quantum-well structure on SiCN/Si(111) substrates, Thin Solid Films 520 (2011) 1084–1090, https://doi.org/10.1016/j.tsf.2011.01.086.
[23] S. Sundaram, Y. El Gmili, R. Puybaret, X. Li, P.L. Bonanno, K. Pantzas, G. Patriarche, P.L. Voss, J.P. Salvestrini, A. Ougazzaden, Nanoselective area growth and characterization of dislocation-free InGaN nanopyramids on AlN buffered Si(111) templates, Appl. Phys. Lett. 107 (2015), https://doi.org/10.1063/1.4931132.
[24] S. Sundaram, R. Puybaret, Y. El Gmili, X. Li, P.L. Bonanno, K. Pantzas, G. Orsal, D. Troadec, Z.H. Cai, G. Patriarche, P.L. Voss, J.P. Salvestrini, A. Ougazzaden, Nanoscale selective area growth of thick, dense, uniform, In-rich, InGaN nanostructure arrays on GaN/sapphire template, J. Appl. Phys. 116 (2014), https://doi.org/10.1063/1.4900531.
[25] W. El Huni, S. Karrakchou, Y. Halfaya, M. Arif, M.B. Jordan, R. Puybaret, T. Ayari, H. Ennakrachi, C. Bishop, S. Gautier, A. Ahaitouf, P.L. Voss, J.P. Salvestrini, A. Ougazzaden, Nanopyramid-based absorber to boost the efficiency of InGaN solar cells, Sol. Energy 190 (2019) 93–103, https://doi.org/10.1016/j.solener.2019.07.090.
[26] M. Arif, J.P. Salvestrini, J. Streque, M.B. Jordan, Y. El Gmili, S. Sundaram, X. Li, G. Patriarche, P.L. Voss, A. Ougazzaden, Role of V-pits in the performance improvement of InGaN solar cells, Appl, Phys. Lett. 109 (2016) 1–5, https://doi.org/10.1063/1.4963817.
[27] E. Matioli, C. Neufeld, M. Iza, S.C. Cruz, A.A. Al-Heji, X. Chen, R.M. Farrell, S. Keller, S. DenBaars, U. Mishra, S. Nakamura, J. Speck, C. Weisbuch, High internal and external quantum efficiency InGaN/GaN solar cells, Appl. Phys. Lett. 98 (2011) 2009–2012, https://doi.org/10.1063/1.3540501.

[28] P. Gibart, B. Beaumont, P. Vennéguès, Epitaxial lateral overgrowth of GaN, in: Nitride Semicond. Handb. Mater. Devices, 2006, pp. 45–106, https://doi.org/10.1002/3527607641.ch2.
[29] E. Monroy, T. Andreev, P. Holliger, E. Bellet-Amalric, T. Shibata, M. Tanaka, B. Daudin, Modification of GaN(0001) growth kinetics by Mg doping, Appl. Phys. Lett. 84 (2004) 2554–2556, https://doi.org/10.1063/1.1705719.
[30] L. Lahourcade, J. Pernot, A. Wirthmüller, M.P. Chauvat, P. Ruterana, A. Laufer, M. Eickhoff, E. Monroy, Mg doping and its effect on the semipolar GaN (11 22) growth kinetics, Appl. Phys. Lett. 95 (2009) 1–4, https://doi.org/10.1063/1.3256189.
[31] S. Karrakchou, S. Sundaram, R. Gujrati, P. Vuong, A. Mballo, H.E. Adjmi, V. Ottapilakkal, W. El Huni, K. Bouzid, G. Patriarche, A. Ahaitouf, P.L. Voss, J. P. Salvestrini, A. Ougazzaden, Monolithic free-standing large-area vertical III-N light-emitting diode arrays by one-step h-BN-based thermomechanical self-lift-off and transfer, ACS Appl. Electron. Mater. 3 (2021) 2614–2621, https://doi.org/10.1021/acsaelm.1c00206.
[32] G.F. Brown, J.W. Ager, W. Walukiewicz, J. Wu, Finite element simulations of compositionally graded InGaN solar cells, Sol. Energy Mater. Sol. Cells 94 (2010) 478–483, https://doi.org/10.1016/j.solmat.2009.11.010.
[33] S. Adachi, Physical Properties of III-V Semiconductor Compounds, Wiley, 1992, https://doi.org/10.1002/352760281X.
[34] A.E. Romanov, T.J. Baker, S. Nakamura, J.S. Speck, Strain-induced polarization in wurtzite III-nitride semipolar layers, J. Appl. Phys. 100 (2006), https://doi.org/10.1063/1.2218385.
[35] W. El-Huni, A. Migan, Z. Djebbour, J.-P. Salvestrini, A. Ougazzaden, High-efficiency indium gallium nitride/Si tandem photovoltaic solar cells modeling using indium gallium nitride semibulk material: monolithic integration versus 4-terminal tandem cells, Prog. Photovoltaics Res. Appl. 24 (2016) 1436–1447, https://doi.org/10.1002/pip.2807.
[36] W. Zhao, L. Wang, J. Wang, Z. Hao, Y. Luo, Theoretical study on critical thicknesses of InGaN grown on (0001) GaN, J. Cryst. Growth 327 (2011) 202–204, https://doi.org/10.1016/j.jcrysgro.2011.05.002.
[37] M. Morales-Masis, S. Martin De Nicolas, J. Holovsky, S. De Wolf, C. Ballif, Low-temperature high-mobility amorphous IZO for silicon heterojunction solar cells, IEEE J. Photovoltaics 5 (2015) 1340–1347, https://doi.org/10.1109/JPHOTOV.2015.2450993.
[38] S.H. Choa, C.K. Cho, W.J. Hwang, K. Tae Eun, H.K. Kim, Mechanical integrity of flexible InZnO/Ag/InZnO multilayer electrodes grown by continuous roll-to-roll sputtering, Sol. Energy Mater. Sol. Cells 95 (2011) 3442–3449, https://doi.org/10.1016/j.solmat.2011.08.001.
[39] E.C. Young, B.P. Yonkee, F. Wu, S.H. Oh, S.P. DenBaars, S. Nakamura, J.S. Speck, Hybrid tunnel junction contacts to III-nitride light-emitting diodes, APEX 9 (2016), https://doi.org/10.7567/APEX.9.022102.
[40] Z. Djebbour, W. El-Huni, A. Migan Dubois, J. Kleider, Bandgap engineered smart three-terminal solar cell: new perspectives towards very high efficiencies in the silicon world, Prog. Photovoltaics Res. Appl. 27 (2019) 306–315, https://doi.org/10.1002/pip.3096.